ISSN 1063-7745, Crystallography Reports, 2024, Vol. 69, No. 1, pp. 38–44. © Pleiades Publishing, Inc., 2024.

CRYSTALLOGRAPHY IN BIOLOGY AND MEDICINE

Dedicated to the 300th anniversary of St. Petersburg State University

Specific Features of the Crystal Structure of Calcium Hydroxyapatite in Native Bone Tissue

A. A. Pavlychev[a,*], X. O. Brykalova[a], A. V. Korneev[a], A. A. Cherny[b], and N. N. Kornilov[b]

[a] *St. Petersburg State University, St. Petersburg, 198504 Russia*

[b] *Vreden National Medical Research Center of Traumatology and Orthopaedics, St. Petersburg, 195427 Russia*

**e-mail: a.pavlychev@spbu.ru*

Received June 8, 2023; revised June 8, 2023; accepted June 29, 2023

Abstract—The effects of physiological and pathogenic factors on the crystal structure of calcium hydroxyapatite $Ca_{10}(PO_4)_6(OH)_2$ in mineralized bone tissues are considered. The unit cell constants of bioapatite, the unit cell deformation, and the crystallite sizes in different groups of bone tissues were analyzed based on the results of X-ray diffraction studies. The main mechanisms responsible for spatial-temporal changes in bone nanostructures were revealed. It was demonstrated that, along with violations of the stoichiometry, an important role is played by the crystallite sizes, estimated as the coherent scattering regions, the number of atoms in which differs by more than two orders of magnitude, and electrostatic interactions between the unbalanced charges of nanocrystallites and hydrated nanolayers of the mineral matrix.

DOI: 10.1134/S1063774523601326

INTRODUCTION

Bone tissue is the most complex material in nature. Its mechanical and physicochemical properties are defined by the interaction of two hierarchically organized subsystems, namely the protein and mineral components. In a saturated aqueous solution, organic molecules create the required biochemical medium, which initiates biologically essential changes in the atomic-molecular architecture of mineralized bone in vertebrate organisms. The specific features of the effect of this medium on the morphology, the growth, the degree of crystallinity, the crystallite size and shape, and the mechanisms responsible for the adaptation of bone tissues to mechanical loads and other external stimuli are poorly known.

Calcium hydroxyapatite ($Ca_{10}(PO_4)_6(OH)_2$, CaOHap) is the principal mineral component of tissue structures of living organisms during their mineralization under physiological conditions [1–4]. The specific features of this mineral are largely due to the flexibility of the atomic structure, allowing the mineral to be easily adapted to external conditions through changes in the stoichiometry, which is closely related to its physicochemical parameters, such as the solubility, elasticity, fragility, and thermal resistance [3–5]. According to the morphological model [1] of bone tissue, coplanar and mosaic assemblies of CaOHap nanocrystallites, located inside and outside collagen fibrils, reproduce the helical shape of these fibrils. An average crystallite is a parallelepiped-shaped block with dimensions of $20 \times 7.5 \times 3.5$ nm^3 containing ~40000 atoms [6]. The sizes and ratios of the sides of such parallelepipeds vary in wide ranges. In the assemblies, the crystallites are separated from one another by hydrated nanolayers of a saturated aqueous solution containing mainly Ca^{2+}, PO_4^{3-}, and OH^- ions trapped in solvation shells [6].

It is known that the parameters of the crystal structure of CaOHap vary in a wide range. The unit cell constant *a* of CaOHap increases from 9.388 Å in adult rat cortical bone [7] to 9.464 Å in the synthesized crystal of CaOHap [8]. The unit cell constant *c* increases from 6.849 Å in newborn rat cortical bone [7] and kidney stones [8, 9] to 6.901 Å in the osteoarthritis (OA)-damaged human femur bone [10]. The ranges of the changes between the observed largest and smallest values of the unit cell constants *a* and *c* are 0.076 and 0.052 Å, respectively, leading both to the volume contraction and expansion of the unit cell to 1.14 and 1.23%, respectively, compared to the unit cell of the stoichiometric crystal. The specificity of the biogenic mineral CaOHap (or bioapatite) is that the replacements of PO_4^{3-} ions with CO_3^{2-} play an important role [8, 11, 12]. These replacements affect the solubility of

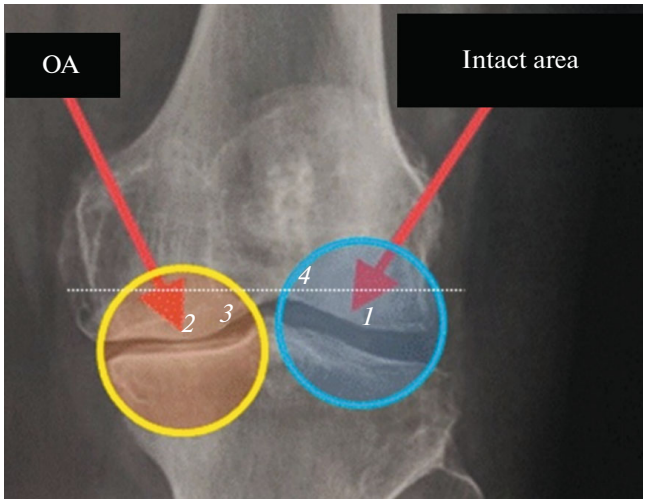

Fig 1. X-ray pattern of an OA-damaged knee joint: (*1*) the intact area, (*2*) the sclerotic bone area, (*3*) the intermediate area, (*4*) the distal side of a saw-cut (dashed line).

the mineral [4] and, as a consequence, the crystallite size. The presence of a carbonate ion leads to an increase in the parameter *c* and a decrease in the parameter *a* [8, 11, 12]. The replacement of the hydroxyl group affects the parameter *a*, while the replacement of Ca^{2+} changes the dimensions of the crystal unit cell according to the ratio of their ionic radii.

Apart from the changes in the elemental composition, there are other factors that cause distortions in the crystal lattice in bone. More than 100 years ago, Julius Wolff hypothesized [13] that the bone structures in vertebrates are determined during the execution of locomotor tasks against the gravitational force. This hypothesis works at the micro- and macrolevels; however, the applicability of this hypothesis to bone nanostructures is poorly understood.

Recently, it was found that the intensity of photoemission current from cortical bone at the Ca^{2+} $L_{2,3}$ absorption edge depends on the orientation of the electric field vector **E** of linearly polarized radiation with respect to the long bone axis [14]. Despite the evident similarity of this effect to the dichroism in crystal optics [15], for example, in $CaCO_3$ crystals [16, 17], which are the main component of the exoskeleton of invertebrates, the two effects are significantly different. Thus, the dichroism of photoabsorption in bone is not directly related to the orientation of the crystallographic axes with respect to the vector **E** but is related to the direction of the resulting gravitational force in the skeleton with respect to **E**. Therefore, this phenomenon reflects the emergent properties of bone and is defined by its hierarchical organization. These properties may be associated not only with the specific orientation of the chemical bonds in bone tissue [14] but also with the deformation of its crystal structure induced by gravitational force. Thus, the transverse orientation of collagen fibrils is more common in bone that experiences compression, whereas their longitudinal orientation predominates in areas that are primarily stretched [1, 18–21].

The question as to whether the Wolff paradigm is applicable to bone nanostructures gives rise to interest in studying the effect of mechanical loads on the crystal structure of native bone, in particular, in analyzing the changes in the crystal structure under OA conditions. The OA-induced systematic spatial-temporal alterations in the degree of crystallinity, the crystallite size, and the unit cell parameters of CaOHap were described in [10, 22, 23]. Taking into account that OA is an age-related disease, the frequency of which increases with age [24, 25], the relationship between OA and the age-related changes in the body at a nanolevel is of particular interest.

In this work, we studied the changes in the structural characteristics of the mineral matrix of bone tissue depending on OA and age factors. For this purpose, we performed X-ray diffraction measurements of two specially selected groups of bone samples in order to separately investigate the OA and age-related changes. The analysis was carried out using, first, the 3D superlattice (3DSL) of "black-nanoboxes-in-muddy-waters" model [6], which relates the energy structure of the valence states of bone and its hierarchical organization, and, second, the concept of spatial-temporal changes in bone nanostructures [7].

MATERIALS AND METHODS

The effect of biogenic and pathogenic factors on the crystal structure of bone was studied using two groups of samples. First group (I) includes saw-cuts of femoral and tibial condyles resected during arthroplasty of the OA-damaged human knee joint. These samples were used to study the effect of the spatial distribution of mechanical loads on bone nanostructures. To illustrate the choice of the samples, the X-ray pattern of the OA-damaged knee joint is shown in Fig. 1. In this figure, the intact area (undamaged bone tissue) is marked as 1, the sclerotic bone area characterized by the maximum mechanical loads, where the cartilage is completely lost, is labeled as 2, and the vicinities of sclerotic bone, where the damaged cartilage comes into contact with mineralized bone is marked as 3. In Fig. 1, the distal side of the saw-cuts corresponding to porous bone is also indicated. The measurements were performed for 10 samples, which made it possible to perform the statistical analysis of the crystal structure parameters for each area.

To prepare bone samples of group I for X-ray diffraction measurements, the saw-cuts were cleaned of cartilage tissue using a gentle mechanical treatment with a scalpel, to a subchondral bone plate. Then, to degrease the cuts and remove the myeloid content from the trabeculae of the spongy layer, the samples

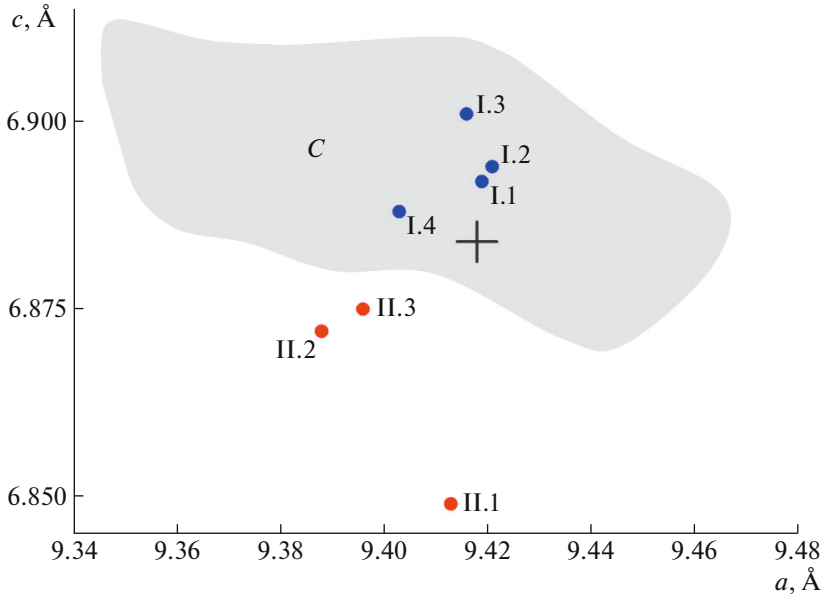

Fig. 2. Unit cell constants a and c for CaOHap. C is the area of the values of the constants a and c of the synthesized crystals, a_{st} and c_{st} in the stoichiometric crystal of CaOHap are marked with an asterisk. The labels I.1–I.4 correspond to the numbers of the areas in Fig. 1; II.1–II.3 indicate the average values of a and c for young, adult, and mature bones, respectively.

were kept for 4 days in a bath containing a 33% aqueous hydrogen peroxide (H_2O_2) solution mixed in a 1 : 1 ratio with hot water (60°C) and supplemented with a 10% aqueous ammonium hydroxide solution (5 mL). This solution was replaced daily. Then the bone samples were soaked in distilled water overnight, changing it every 6–9 h, to complete the chemical cleaning of the cuts.

The second group of samples (II) was used to analyze age-related changes. This group includes samples of the cortical layer of the middle-third of the femur, tibia, and humeri of six (for each age) healthy outbred albino newborn rats with a weight of 50–80 g, adult rats (120–150 g), and mature rats (250–280 g). To perform the measurements, the cortical layer was carefully cleaned of soft tissues, washed in a physiological solution, dried with filter paper, and ground in a porcelain mortar to a grain size of ~1 μm.

All bone samples were prepared at the Vreden National Medical Research Center of Traumatology and Orthopedics. The measurements were performed at the Resource Centre "X-ray Diffraction Studies" of the Research Park of the St. Petersburg State University using a Bruker D8 Discover X-ray diffractometer equipped with a copper anode and a 4-fold germanium monochromator in the range $2\theta = 5°–100°$. The degree of crystallinity, the unit cell parameters, and the sizes of coherent scattering regions of CaOHap in bone samples were calculated by the Rietveld method using the TOPAS 5 program.

COMPARATIVE ANALYSIS OF CHANGES IN THE CRYSTAL STRUCTURE

It was demonstrated that the mineralized phase in all samples is formed by hexagonal CaOHap. The degree of crystallinity, the superlattice periodicity, the sizes of crystallites, violations of their stoichiometry, distortions of the unit cell constants, the degree of crystallinity, and crystallite sizes demonstrate systematic concerted spatial-temporal changes [7].

In Fig. 2 the unit cell constants a and c of CaOHap, determined for samples of groups I and II, are marked by dots. For comparison, Fig. 2 presents the area C (shaded region), which includes numerous values of the constants a and c of the hexagonal CaOHap crystals synthesized by different methods in the study [8]. The asterisk indicates the position of $a_{st} = 9.418$ Å and $c_{st} = 6.884$ Å [26] in the stoichiometric crystal of CaOHap.

As can be seen in Fig. 2, there are differences in the positions of the average a and c values in groups I and II and these positions depend on the spatial distribution of mechanical loads and the age. It should be noted that $c > c_{st}$ in I and $c < c_{st}$ in II; almost for all samples, $a < a_{st}$; in group I the constants a and c are located in the area C; in group II, outside this area. Due to the location of the constants a and c inside the area C, the conclusions drawn for the synthesized crystals can be used in the analysis of the crystal structure of these samples.

Taking into account that the changes $\Delta c_{i,j}$ between the ith and jth areas are larger than the root-mean-squares deviations σ_c [10], it can be said that there are

Table 1. Structural characteristics of mineralized bone tissue in different areas for samples of group I

	CaOHap*	I.1	I.3	I.2	I.4
a, nm	0.9418	0.9419	0.9416	0.9421	0.9403
c, nm	0.6884	0.6892	0.6901	0.6894	0.6888
v, %**	0	0.14	0.20	0.21	−0.15
δ, %***	0	0.11	0.27	0.11	0.22
D, %	100	65	42	85	90
L, nm		15	16	11	20
N		1.4×10^5	1.7×10^5	5.5×10^4	3.3×10^5

* Stoichiometric CaOHap (JCPDS no. 09-0432). ** $v = \dfrac{V_{\text{bone}} - V_{\text{ap}}}{V_{\text{ap}}}$. *** $\delta = \dfrac{(c/a)_{\text{bone}} - (c/a)_{\text{ap}}}{(c/a)_{\text{ap}}}$.

systematic spatial changes in the constant c, which can be related to the spatial changes in the concentration (w) of $[CO_3]^{2-}$ ions replacing $[PO_4]^{3-}$. Based on the linear dependence of the constant c on w, which was found in [8], we determined the concentrations of $[CO_3]^{2-}$ ions in different areas of OA-damaged femoral bone.

The minimum concentration of $[CO_3]^{2-}$ ions (carbonization) was found on the distal side of saw-cuts in the area I.4, and the maximum carbonization was observed in the area I.3 (Fig. 1), i.e., on the proximal side, at the interface between the damaged cartilage and the mineral. Inside the sclerotic bone area (I.2) characterized by the maximum mechanical loads, the concentration of $[CO_3]^{2-}$, like in the intact area (I.1), is significantly lower. The revealed relationship between the changes in c and w for bone samples is consistent with the photoelectron spectroscopy data [10]. Actually, the analysis of the shape of the Ca^{2+} $2p^{-1}_{3/2,1/2}$ photoelectron line in [8] demonstrated that the composition of this line in the areas I.2 and I.3 is significantly complicated due to the appearance of new non-apatite states of Ca^{2+}, the maximum contribution of which is observed in the area I.3. For comparison, it should be noted that the contribution of apatite states of Ca^{2+} is ~100% in I.1 and I.4.

Unlike the constant c, the constant a changes only slightly in going from one area to another, resulting in the uniaxial deformation of the crystal unit cell. Table 1 gives the values of the parameters a and c, the volume v and uniaxial δ compression of the unit cell, the degree of crystallinity D, and the linear sizes L of crystallites in different areas of group I. The negative values of v correspond to the volume compression of the unit cell; the negative values of δ, to the compression (flattening) along the c axis compared to the unit cell of the stoichiometric crystal.

An analysis of the constants a and c for group II demonstrated the systematic changes in these constants in the areas II.1 → II.2 → II.3. The tendency of these changes suggests that they are related to the effect of calcium vacancies [7]. However, unlike group I, it is difficult to obtain the quantitative data on their concentration because the measured positions of a and c are outside the area C. The structural characteristics of bone samples of group II are summarized in Table 2.

The question remains open as to why $a, c \notin C$ in samples of group II, whereas $a, c \in C$ in group I. The search for the answer to this question is an important issue. It can be suggested that, apart from violations of the stoichiometry, there are other mechanisms responsible for the effects on the unit cell of CaOHap in bone tissue, which play a more important role in group II.

A comparison of the data in Tables 1 and 2 shows that the linear sizes L of crystallites (coherent scattering regions) in group II are many times smaller compared to those in group I. By evaluating the number of atoms N in crystallites, we find that these values differ by more than two orders of magnitude. In II.1 (young bone), $N < 2 \times 10^3$; $N > 300 \times 10^3$ in I.4 (distal side of saw-cuts) (Tables 1 and 2). These significant differences affect the electronic and atomic structure of crystallites and lead to changes in the mechanisms responsible for the stability and structural-functional properties of crystallites at the nanolevel [27]. It should also be noted that the constants a and c are most far from the area C for samples II.1, which contain the minimum number of atoms N.

According to the 3DSL model, the energy of valence states in the mineral matrix is lower compared to the band energy E_n in the CaOHap crystal [6]. The shift ΔE_n depends on the crystallite sizes and the thickness of the hydrated layers in assemblies:

$$\Delta E_n = E_{\text{bone}} - E_n \approx 2\gamma E_n \frac{d}{L}, \quad (1)$$

where L and d are the effective sizes of crystallites and hydrated layers, respectively, γ (≈D) is the fraction of atoms that form a superlattice [6]. This relation was derived assuming that the energy structure of the crystallite can be approximately characterized in terms of the band model; crystallites are in essence extended electrically neutral unit cells of CaOHap that form

Table 2. Structural characteristics of mineralized bone tissues of different ages for samples of group II

	CaOHap*	II.1	II.2	II.3
a, nm	0.9418	0.9413	0.9388	0.9396
c, nm	0.6884	0.6849	0.6872	0.6875
v, %**	0	−0.61	−0.81	−0.64
δ, %***	0	−0.46	0.14	0.10
D, %	100	84	97	96
L, nm		3.5	4.6	4.5
N		1.8×10^3	4.0×10^3	3.8×10^3

* Stoichiometric CaOHap (JCPDS no. 09-0432).** $v = \frac{V_{bone} - V_{ap}}{V_{ap}}$. *** $\delta = \frac{(c/a)_{bone} - (c/a)_{ap}}{(c/a)_{ap}}$.

a three-dimensional superlattice (a mesocrystal [28]); the dielectric properties of the hydrated layers can be ignored. As can be seen from Eq. (1), a decrease in L leads to an increase in the difference between the energy structures of the crystal and the crystallite. On the contrary, $\Delta E_n \to 0$ and the differences are diminished with increasing L.

As L decreases, the requirement of electrical neutrality of the unit cell becomes less stringent because additional interactions occur between atoms in crystallites and hydrated layers. By considering the mineral matrix as a 3D superlattice, it can be suggested that the compensation of the charge should occur in the superunit S, which involves the crystallite and adjacent hydrated layers [7]. In this case

$$\int_S \frac{d}{dr} Q(r)\, dr \equiv 0, \qquad (2)$$

where $Q(r)$ is the distribution of the electrical charge in the assembly. The nature of the charge of the crystallite is related to the violations of the stoichiometry due to the replacement of atoms and the formation of vacancies. This conclusion is consistent with the assumption of an excessive negative charge on the crystallites [7], which has the maximum value in young bone (II.1) and decreases with age. This charge is compensated by the positive charge of hydrated layers. In terms of this model, there are additional electrostatic forces in the superunit S, resulting in its deformation.

An analysis of this deformation depending on the physiological and pathogenic factors allows a deeper understanding of the nature of spatial-temporal changes in the crystal lattice in bone tissue. Let us consider its characteristics as a function of the parameter τ defining it as $\tau \equiv \frac{t}{T}$. For group I, t is the time from the onset of OA disease, T is the average duration of the disease, ultimately leading to the complete loss of the cartilage. For group II, t is the age of bone, T is the average lifetime of the organism. The parameter τ characterizes a combination of changes in the atomic-molecular architecture of bone at this point in time t. Figure 3 shows the changes in the characteristics of the crystal lattice depending on τ for groups I (black lines) and II (grey lines). The parameters in the intact area (I.1) and for young bone (II.1) were correlated to $\tau \approx 0$; the parameters in I.3 (partially damaged cartilage) and II.2 (adult bone), to $\tau \approx 0.5$; the parameters in I.2 (sclerotic bone) and II.3 (mature bone), to $\tau \approx 1$.

The plots of a, c, v, and δ versus τ are shown in Fig. 3. It is seen that the characteristics of the crystal lattice and the tendencies of their changes are significantly different. In group I the unit cell volume is larger, the unit cell is stretched along the c axis and shows small changes in the constant a. On the contrary, in group II the unit cell volume is contracted, and the unit cell is flattened along the c axis. The pronounced uniaxial deformation of the unit cell depending on the age demonstrates that investigations of the dichroism of photoabsorption are promising for the visualization of age-related changes in bone nanostructures.

Let us pay attention to the behavior of the constants a and c in the range $0.5 < \tau < 1$ in group I. This range corresponds to mechanical loads in the case of the complete absence or a strong damage of the cartilage. As can be seen in Fig. 3, the constant a increases and the constant c decreases in this range. Based on the data in Table 1, $\varkappa = -\frac{\Delta a c}{a \Delta c} \approx 0.5$, which is similar to the Poisson's ratio for apatite. This result suggests that the changes in the parameters of the crystal structure of CaOHap in the final stage of OA may be due to mechanical loads, which is indicative of the applicability of the Wolff paradigm to bone nanostructures. Therefore, along with the violations of the stoichiometry, the size effects, and additional electrostatic interactions in assemblies, the changes in the crystal structure in bone tissue are determined by mechanical loads in the body during the execution of locomotor tasks.

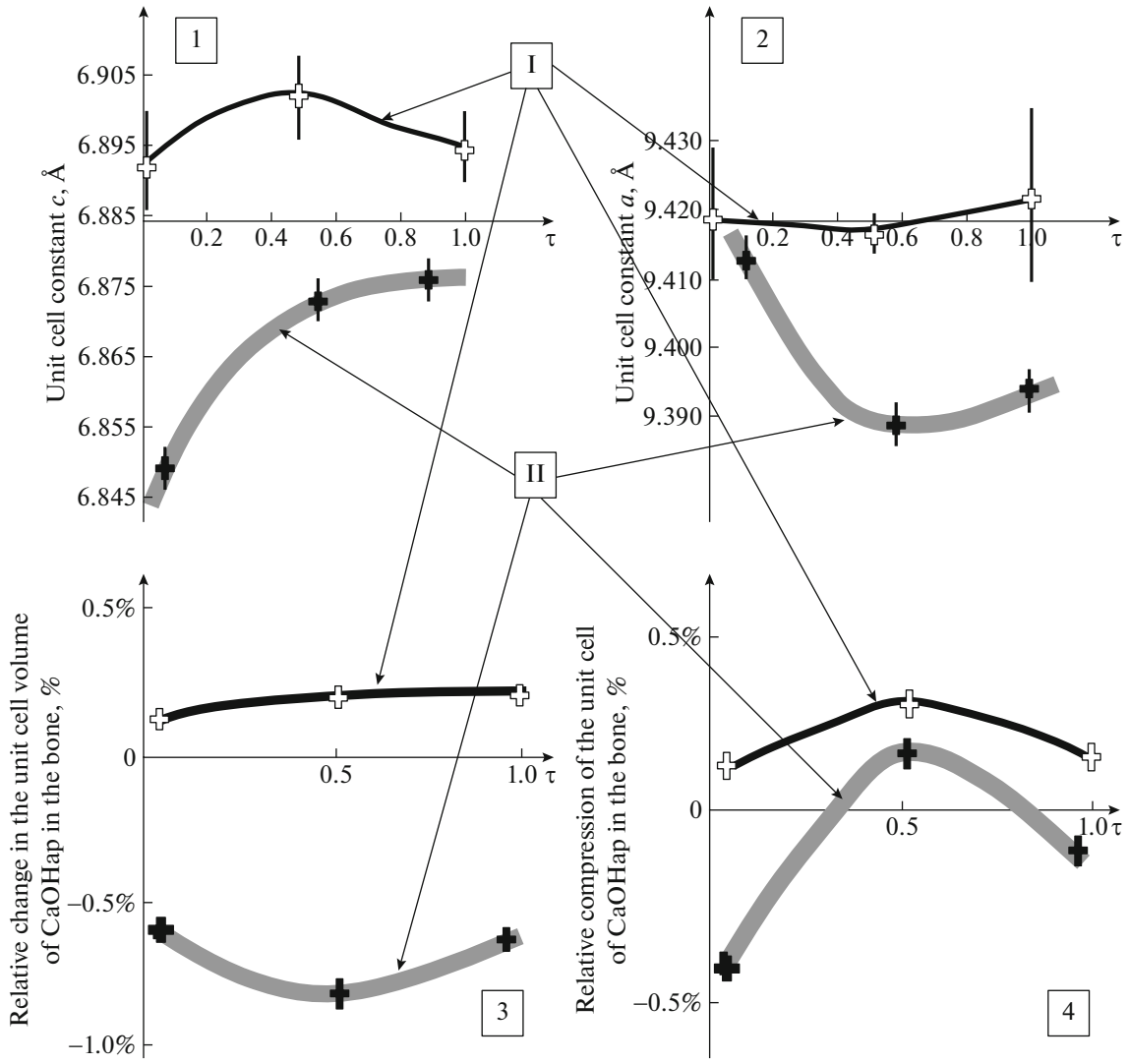

Fig. 3. Spatial-temporal changes in the constants *a* and *c*, the bulk and uniaxial compression of the unit cell of CaOHap depending on the parameter τ. The symbols I and II indicate the corresponding group of samples.

CONCLUSIONS

The unit cell constants of calcium hydroxyapatite, the specific features of the unit cell deformations, and the crystallite sizes in bone tissues were analyzed depending on the physiological and pathogenic conditions. The systematic spatial-temporal distortions of the unit cell parameters caused by OA damage and age-related changes in mineralized bone tissue were revealed. It was found that, along with violations of the stoichiometry, an important role in the distortions of the crystal structure of native bone is played by the crystallite sizes, additional electrostatic interactions in the mineral matrix, and the distribution of mechanical loads during the execution of locomotor functions. It was demonstrated that the number of atoms, that form coherent scattering regions in bone tissue, can differs by more than two orders of magnitude (less than 2×10^3 in young bone and more than 300×10^3 in porous bone). Additional electrostatic interactions occur due to the nonequilibrium charge distribution in crystallites and hydrated layers. Further investigations of changes in the crystal structure of mineralized bone hold promise for the development of new methods for the control of age-related processes, treatment and regeneration of damaged bone tissues and also for the development of new biotechnological tools for the design of environmentally benign osteomimetic materials for the conversion and accumulation of electrical energy.

FUNDING

The study was financially supported by the Russian Science Foundation (project no. 23-29-00172). The measurements were carried out using the equipment of the Resource Centres “Diagnostics of Functional Materials for Medi-

cine, Pharmacology and Nanoelectronics" and "X-ray Diffraction Studies" of the Research Park of the St. Petersburg State University.

ETHICS APPROVAL AND CONSENT TO PARTICIPATE

All applicable international, national, and/or institutional guidelines for the care and use of animals were followed.

CONFLICT OF INTEREST

The authors of this work declare that they have no conflicts of interest.

REFERENCES

1. Yu. I. Denisov-Nikolskii, S. P. Mironov, N. P. Omeljanenko, et al., *Actual Problems of Theoretical and Clinical Osteoartrology* (JSC "Printing-house "News," Moscow, 2005).
2. A. A. Doktorov and Yu. I. Denisov-Nikolskii, Bull. Exp. Biol. Med. **119** (1), 61 (1993).
3. J. D. Pasteris, B. Wopenka, and E. Valsami-Jones, Elements **4**, 97 (2008).
4. B. Wopenka and J. D. Pasteris, Mater. Sci. Eng. C **25** (2), 131 (2005).
5. S. N. Danil'chenko, Vestn. SumDU, Ser.: Fiz., Mat., Mekh. **2**, 33 (2007).
6. A. A. Pavlychev, A. S. Avrunin, A. S. Vinogradov, et al., Nanotechnology **27**, 504002 (2016). https://doi.org/10.1088/27/50/504002
7. X. O. Brykalova, N. N. Kornilov, and A. A. Pavlychev, J. Mater. Chem. A **10**, 22686 (2022). https://doi.org/10.1039/D2TA02340G
8. O. V. Frank-Kamenetskaya, A. B. Kol'tsov, M. A. Kuz'mina, et al., J. Mol. Struct. **992**, 9 (2011). https://doi.org/10.1016/j.molstruc.2011.02.013
9. O. V. Frank-Kamenetskaya, *Minerals As Advanced Materials* (Springer, Berlin, 2008), p. 241.
10. A. A. Pavlychev, X. O. Brykalova, A. A. Cherny, et al., Crystals **13**, 381 (2023). https://doi.org/10.3390/cryst3030381
11. D. G. A. Nelson and J. D. B. Featherstone, Calcif. Tissue Int. **34**, 69 (1982).
12. M. Vignoles, G. Bonel, D. W. Holcomb, et al., Calcif. Tissue Int. **43**, 33 (1988).
13. J. Wolff, *Das Gesetz der Transformation der Knochen* (Hirschwald, Berlin, 1892).
14. A. S. Konashuk, X. O. Brykalova, N. N. Kornilov, et al., Emergent Mater. **3**, 515 (2020). https://doi.org/10.1007/s42247-020-00105-1
15. M. Born and E. Wolf, *Principles of Optics* (Pergamon, Oxford, 1964).
16. R. A. Metzler and P. Rez, J. Phys. Chem. B **118**, 6758 (2014). https://doi.org/10.1021/jp503565e
17. P. Krüger and C. R. Natoli, J. Phys: Conf. Ser. **712**, 012007 (2016). https://doi.org/10.1088/1742-6596/712/1/012007
18. J. K. Kalmey and C. O. Lovejoy, Bone **31**, 327 (2002).
19. A. Boyde and C. M. Riggs, Bone **11**, 35 (1990).
20. S. Carando, M. Portigliatti-Barbos, A. Ascenzi, et al., Bone **12**, 265 (1991).
21. S. I. Hong, L. Hasche, and S. Bowland, Gerontologist **49**, 1 (2009). https://doi.org/10.1093/geront/gnp006
22. X. O. Brykalova, N. N. Kornilov, Y. A. Rykov, et al., J. Phys. Chem. Lett. **11**, 7839 (2020). https://doi.org/10.1021/acs.jpclett.0c01722
23. X. O. Brykalova, N. N. Kornilov, A. A. Cherny, et al., Eur. Phys. J. D **73**, 113 (2019). https://doi.org/10.1140/epjd/e2019-100114-8
24. *Joint: Morphology, Clinic, Diagnosis, Treatment,* Ed. by V. N. Pavlova et al. (OOO Izdatel'stvo "Meditsinskoe Informatsionnoe Agentstvo," Moscow, 2011).
25. B. Yucesoy, L. E. Charles, B. Baker, and C. M. Burchfiel, Work **50**, 261 (2015). https://doi.org/10.3233/WOR-131739
26. JCPDS No. 09-0432.
27. A. S. Avrunin, A. A. Pavlychev, Yu. I. Denisov-Nikolskij, et al., Morphology **150** (5), 77 (2016).
28. S. Rui Qi and H. Cölfen, Adv. Mater. **22**, 1301 (2010). https://doi.org/10.1002/adma.200901365

Translated by T. Safonova